Supporting Information

A *meta*-link isomer of ITIC: influence of aggregation patterns on open-circuit voltage in organic solar cells

Kai Wang,[a] Seihou Jinnai,*[a,b] Kaito Uesaka,[c] Akira Yamakata,*[c,d,e] and Yutaka Ie*[a,b]

[a] The Institute of Scientific and Industrial Research (SANKEN), Osaka University, 8-1 Mihogaoka, Ibaraki, Osaka 567-0047
[b] Innovative Catalysis Science Division Institute for Open and Transdisciplinary Research, Osaka University, 2-1 Yamadaoka, Suita, Osaka 565-0871
[c] Graduate School of Natural Science & Technology, Okayama University, 3-1-1 Tsushima-naka, Okayama 700-8530
[d] Research Institute for Interdisciplinary Science, Okayama University, 3-1-1 Tsushima-naka, Okayama 700-8530, Japan
[e] Institute for Aqua Regeneration, Shinshu University, 4-17-1 Wakasato, Nagano-shi, Nagano 380-8553, Japan

*Corresponding author: Email: jinnai@sanken.osaka-u.ac.jp; yamakata@okayama-u.ac.jp; yutakaie@sanken.osaka-u.ac.jp

Table of Contents

Supplemental figures and tables

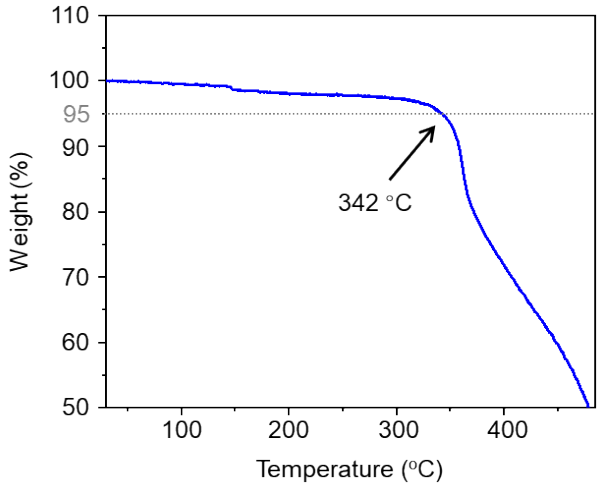

Fig. S1 TGA profile of **im-ITIC**.

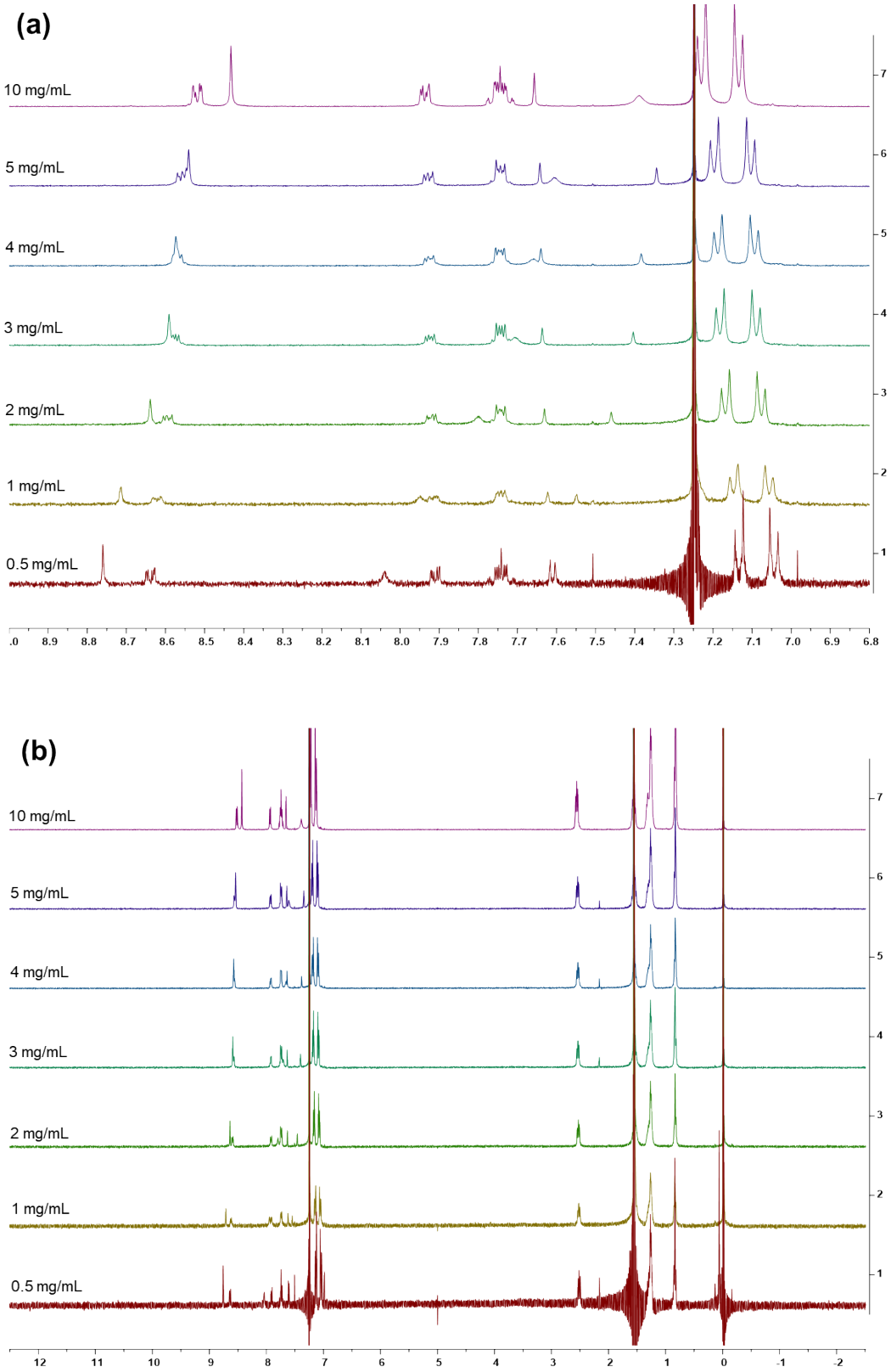

Fig. S2 ^{1}H NMR (400 MHz, $CDCl_3$) spectra for different concentrations of **im-ITIC**. (a) aromatic region and (b) full spectra.

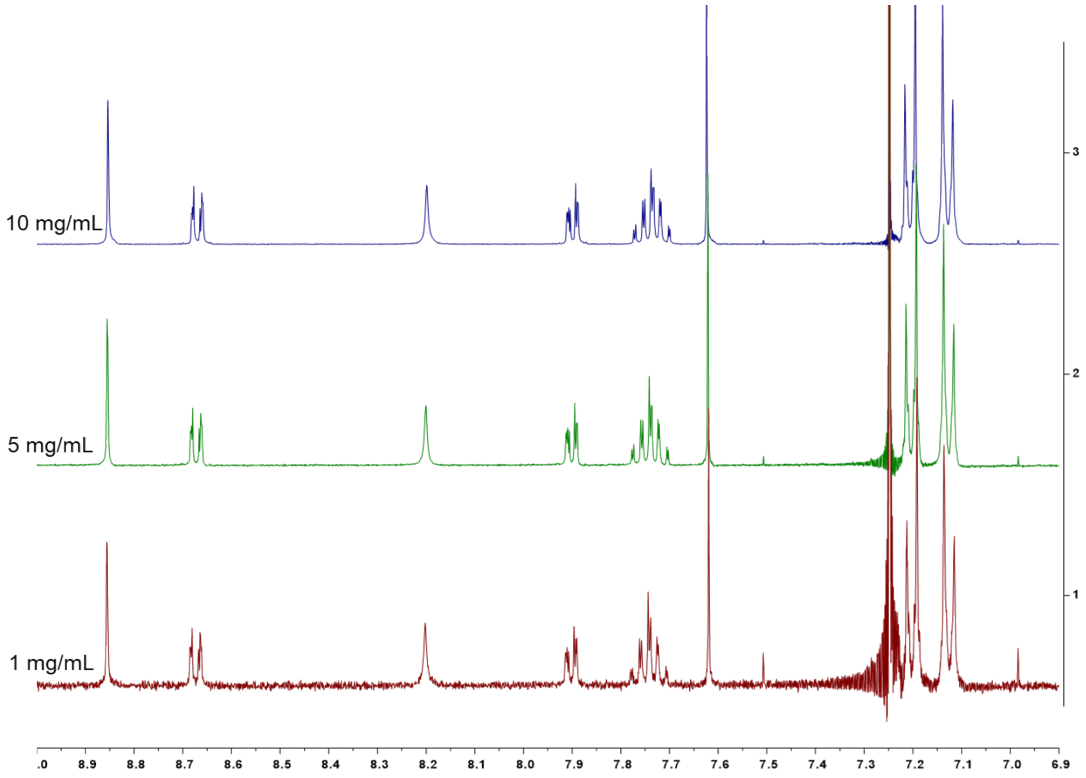

Fig. S3 Concentration-dependent ^{1}H NMR spectra of the aromatic region for **ITIC** in $CDCl_3$ at 20 °C.

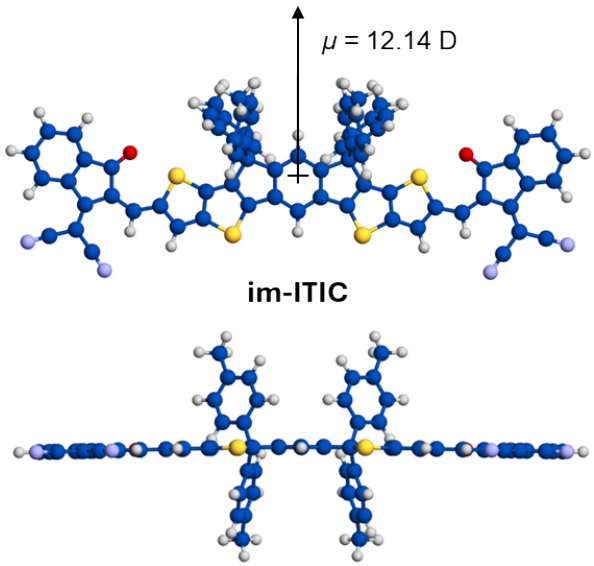

Fig. S4 Top and side views of the optimized structures for **im-ITIC**. μ represents the dipole moment.

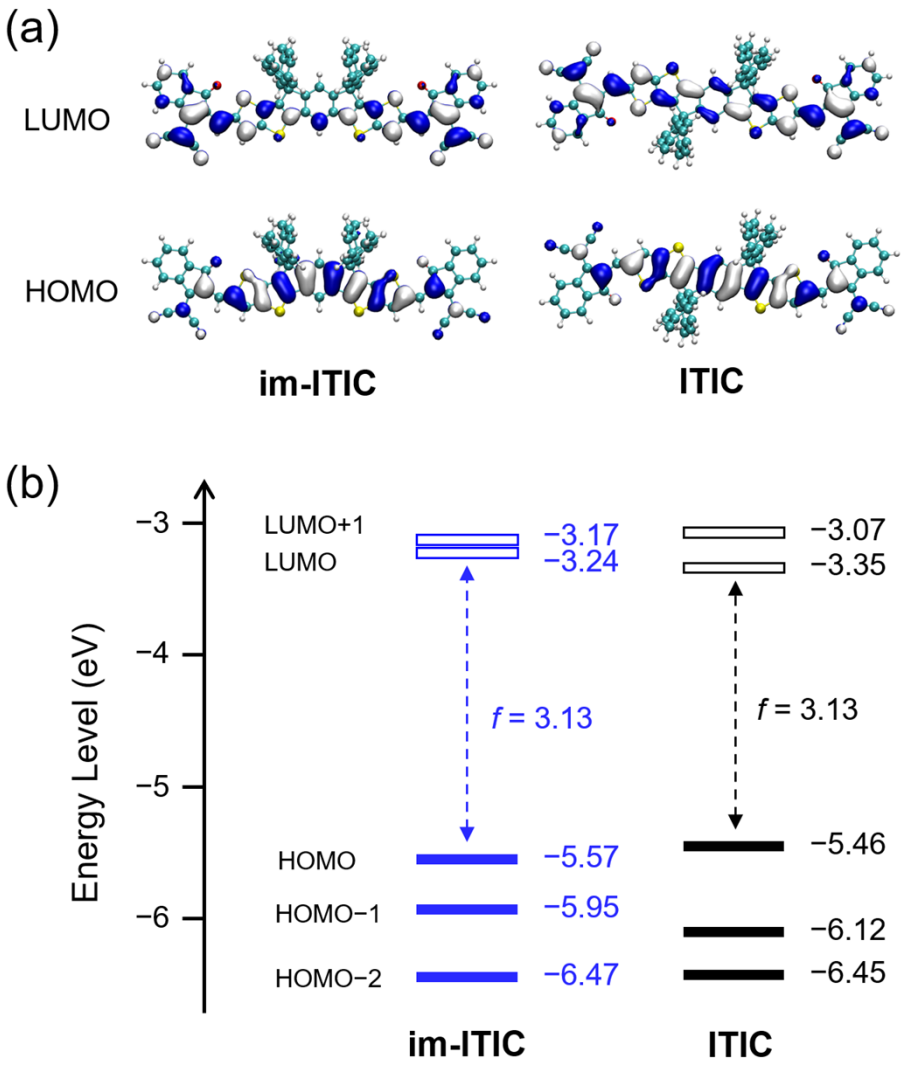

Fig. S5 (a) Distribution of HOMO and LUMO orbitals. (b) Energy level of the molecular orbitals.

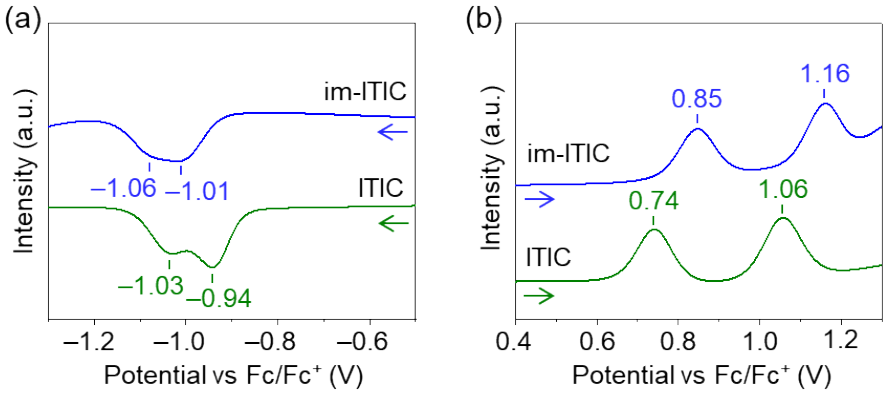

Fig. S6 DPV results of **im-ITIC** and **ITIC** for (a) negative and (b) positive scans in *o*-DCB/CH_3CN (5/1) containing 0.1 M $TBAPF_6$.

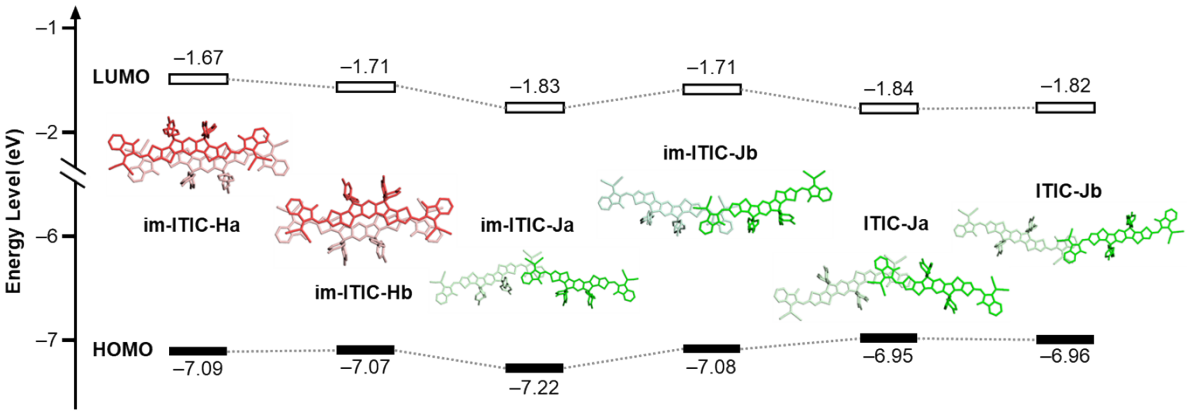

Fig. S7 Energy levels of HOMO and LUMO for **im-ITIC** and **ITIC** by different aggregation pairs. All calculations were performed at the ωB97XD/6-31G(d,p) level.

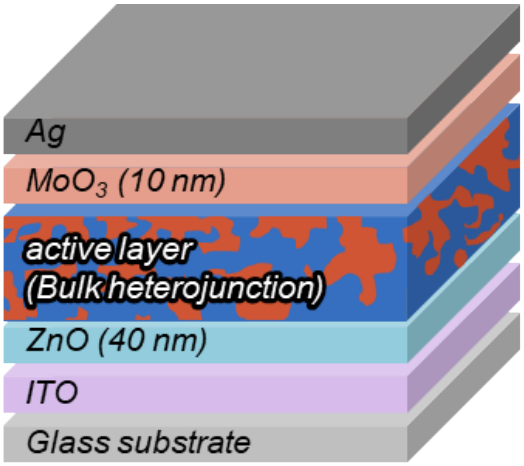

Fig. S8 Device structure for BHJ-OSC devices.

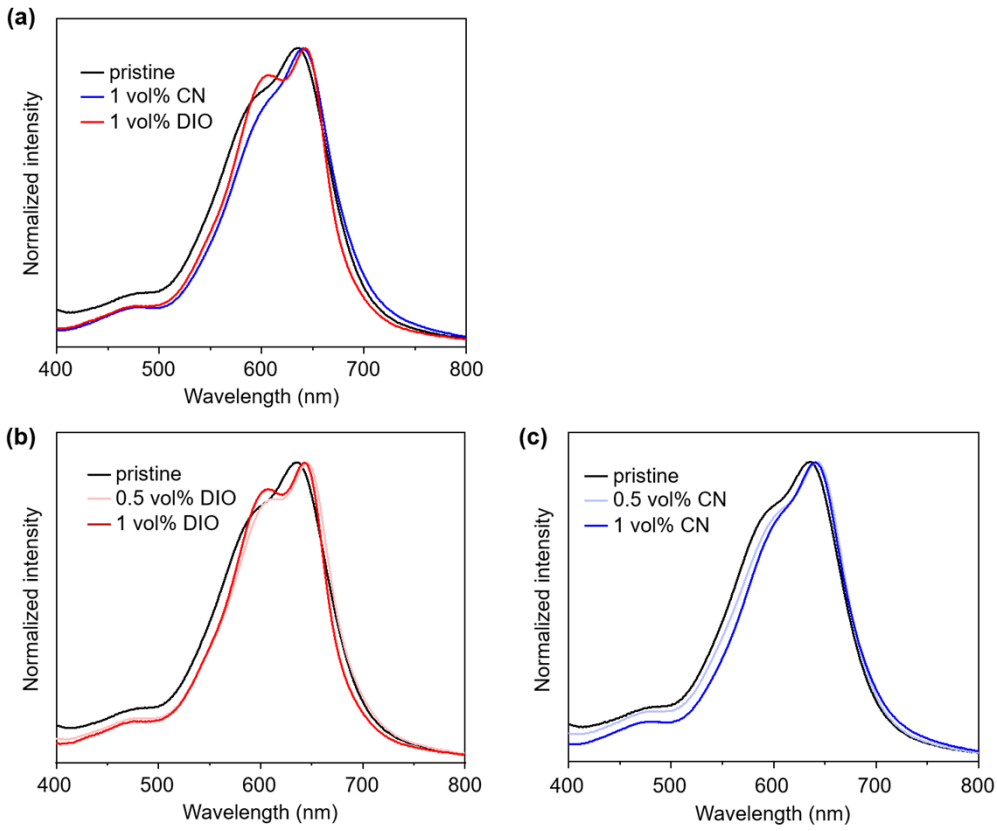

Fig. S9 (a) UV-vis absorption spectra of **im-ITIC** without additive, with 1 vol% CN, and with 1 vol% DIO. UV-vis absorption spectra of **im-ITIC** with different content of (b) DIO and (c) CN.

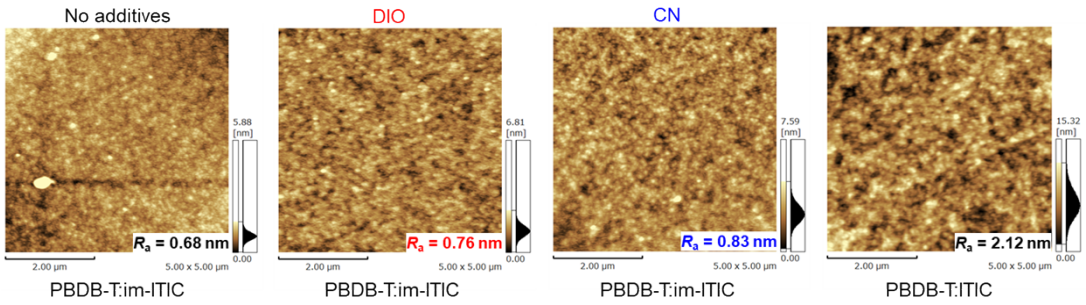

Fig. S10 AFM height images of the PBDB-T:**im-ITIC** blend films with different additives and the PBDB-T:**ITIC** blend film.

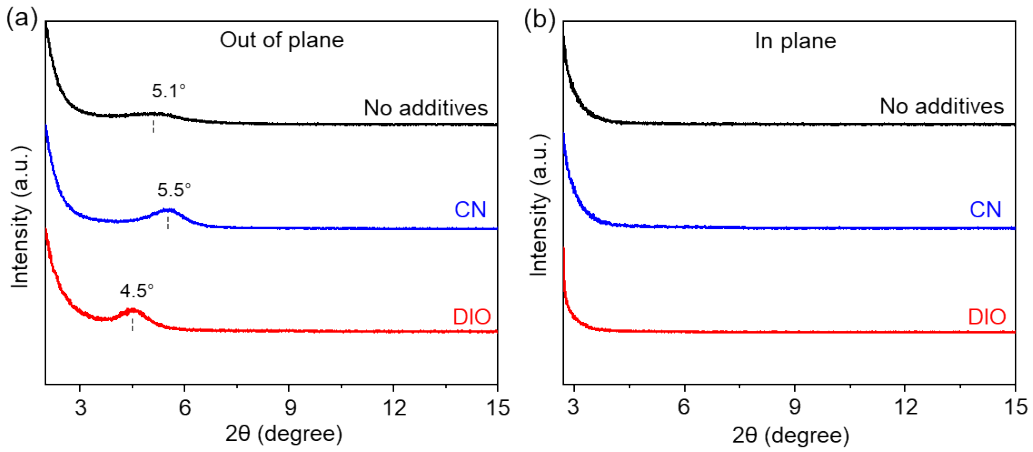

Fig. S11 Out-of-plane (a) and in plane (b) X-ray diffractograms of films with different additives.

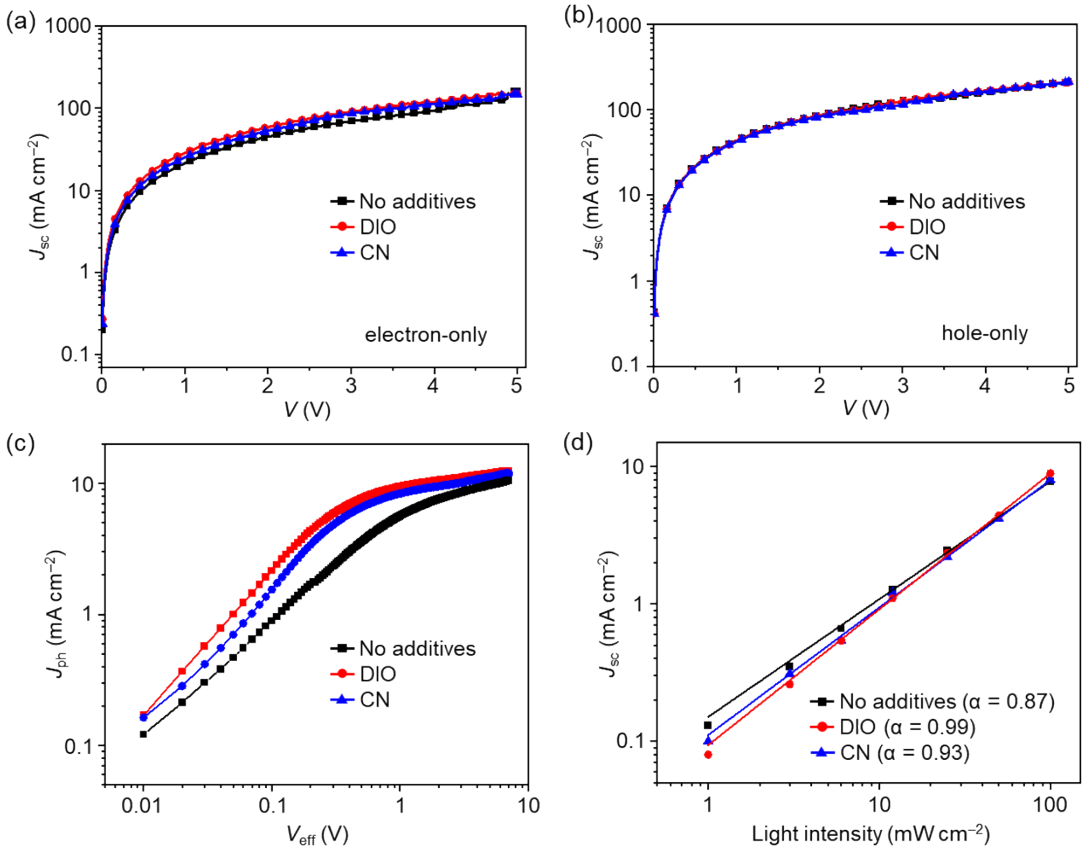

Fig. S12 *J*–*V* plots of (a) electron-only and (b) hole-only devices based on the PBDB-T:**im-ITIC** blend films with different additives; (c) $J_{ph} - V_{eff}$ curves of devices based on the PBDB-T:**im-ITIC** blend films with different additives; (d) light intensity dependent J_{sc} of devices based on the PBDB-T:**im-ITIC** with different additives.

Table S1. Hole and electron mobilities of the PBDB-T:**im-ITIC** films with different additives.

Additives	μ_h (cm²/V·s)[a]	μ_e (cm²/V·s)[b]
-	2.51×10^{-5}	0.92×10^{-5}
DIO	2.52×10^{-5}	0.99×10^{-5}
CN	2.52×10^{-5}	0.97×10^{-5}

[a] ITO/PEDOT:PSS/PBDB-T:acceptor/MoO_3/Ag. [b] ITO/ZnO/PBDB-T:acceptor/Ca/Ag.

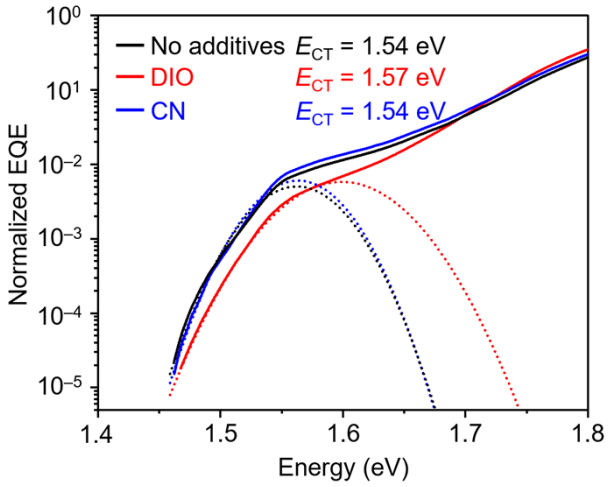

Fig. S13 (a) Normalized EQE spectra of the PBDB-T:**im-ITIC** blend films with different content of additives. The dashed plots indicate the fitting results to obtain E_{CT}.

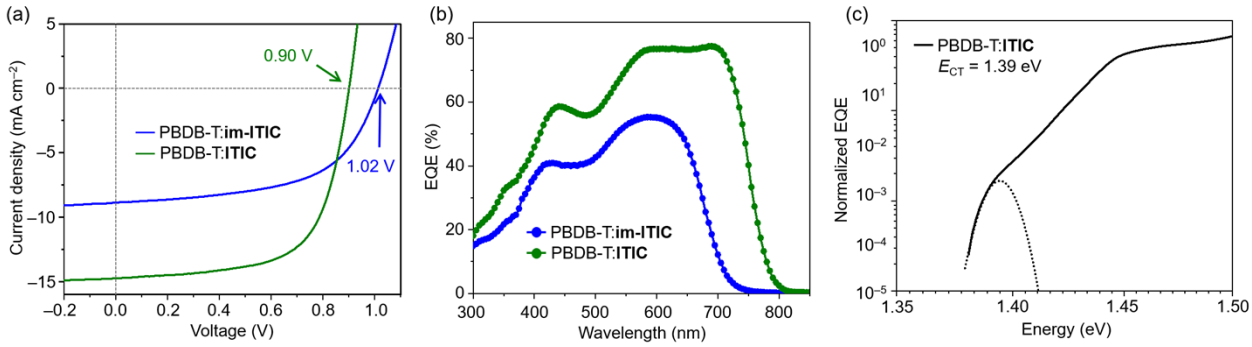

Fig. S14 (a) *J*–*V* curves, and (b) EQE spectra of best-performing OSCs of **im-ITIC** and **ITIC.** (c) Normalized EQE for the PBDB-T:**ITIC** blend film. The dashed plot indicates the fitting results to obtain E_{CT}.

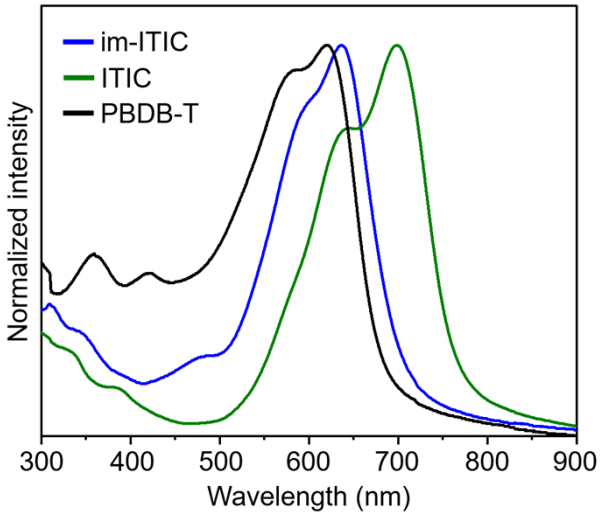

Fig. S15 UV-vis absorption spectra of im-ITIC, ITIC and PBDB-T in pristine films.

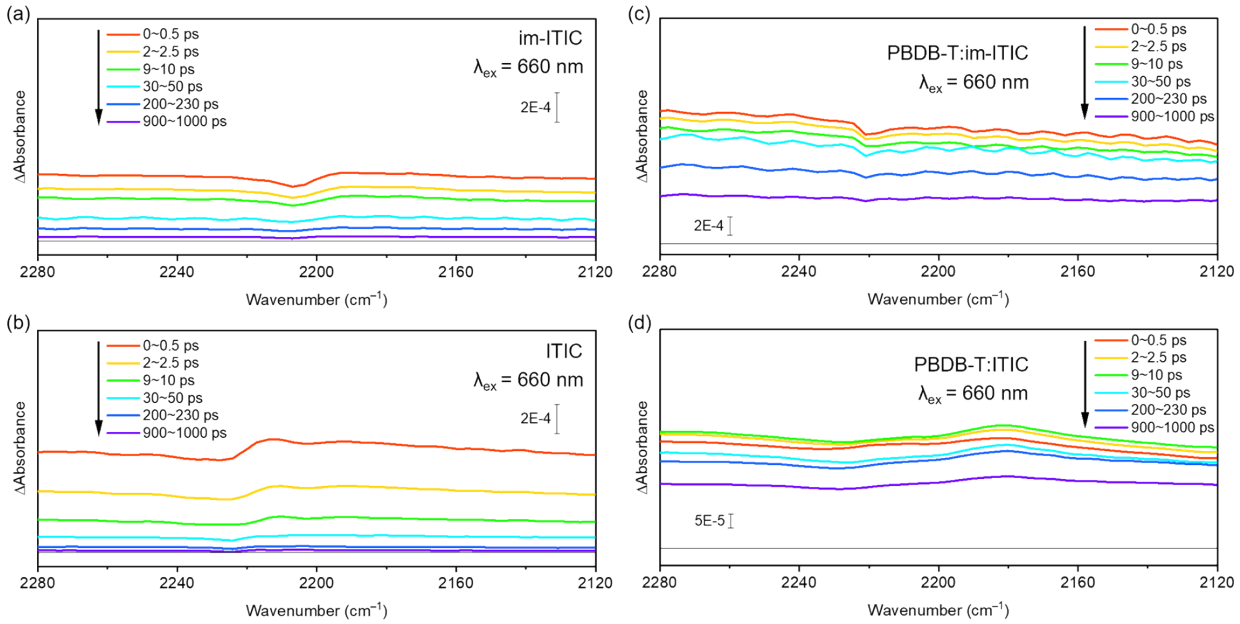

Fig. S16 Transient IR spectra of NFAs after pump pulse irradiation. Pristine **im-ITIC** (a) and **ITIC** (b). Additionally, the NFA domain in the blend film with PBDB-T is photoexcited by the same 660 nm pump pulse (panels c–d).

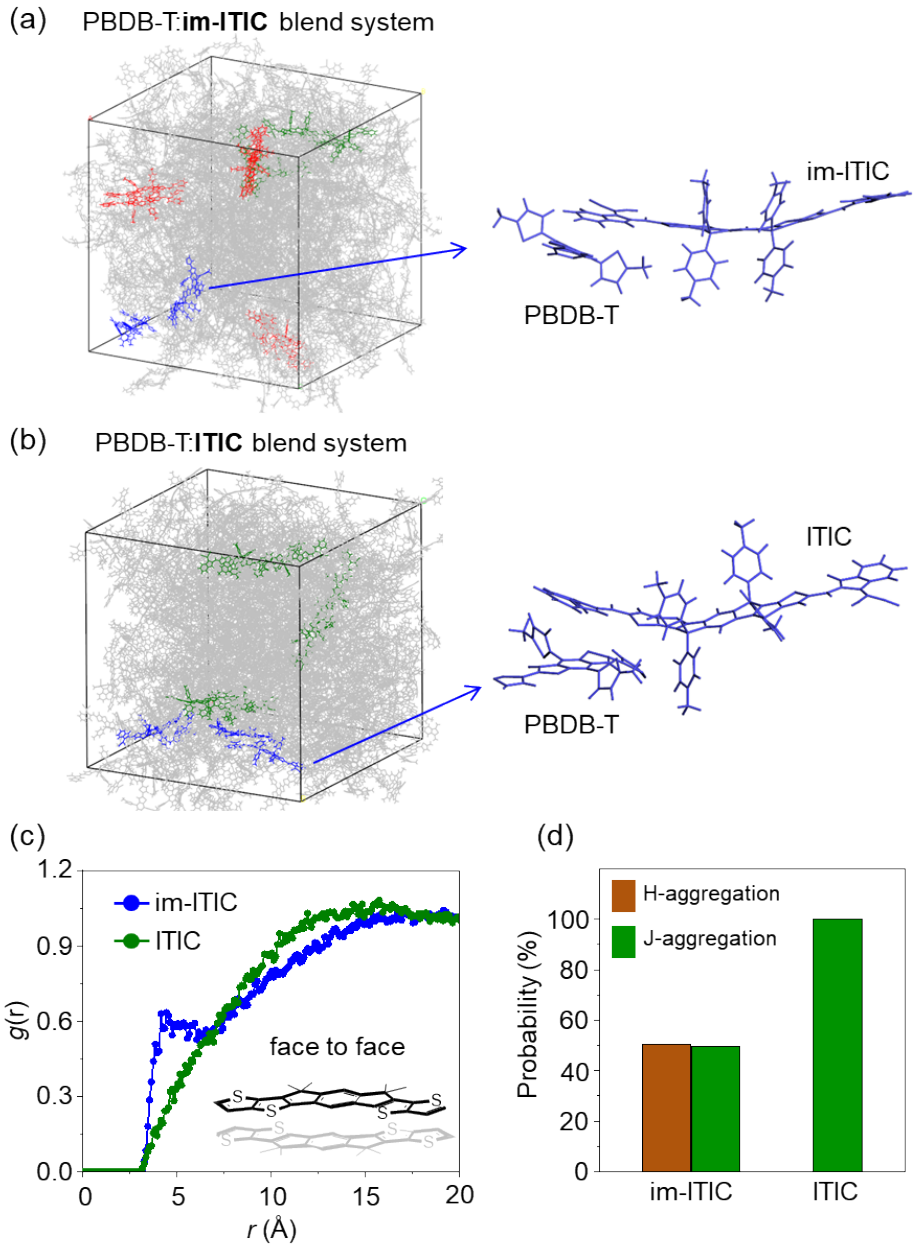

Fig. S17 (a) and (b) Snapshots (left) and examples of stacking modes (right) from the MD results of PBDB-T:**im-ITIC** and PBDB-T:**ITIC**-based blend systems. (c) Radial distribution function data for blend systems. (d) Probability of different aggregations in blend systems.

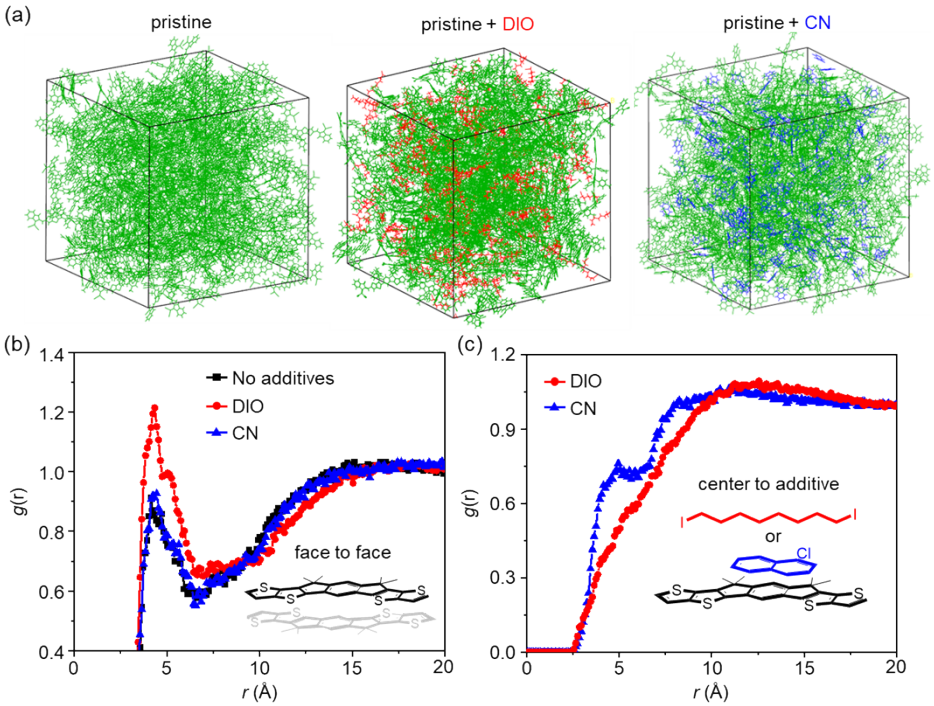

Fig. S18 (a) Snapshots from the MD results of **im-ITIC**-based pristine systems with different additives. (b) and (c) Radial distribution function data for **im-ITIC**-based pristine systems.

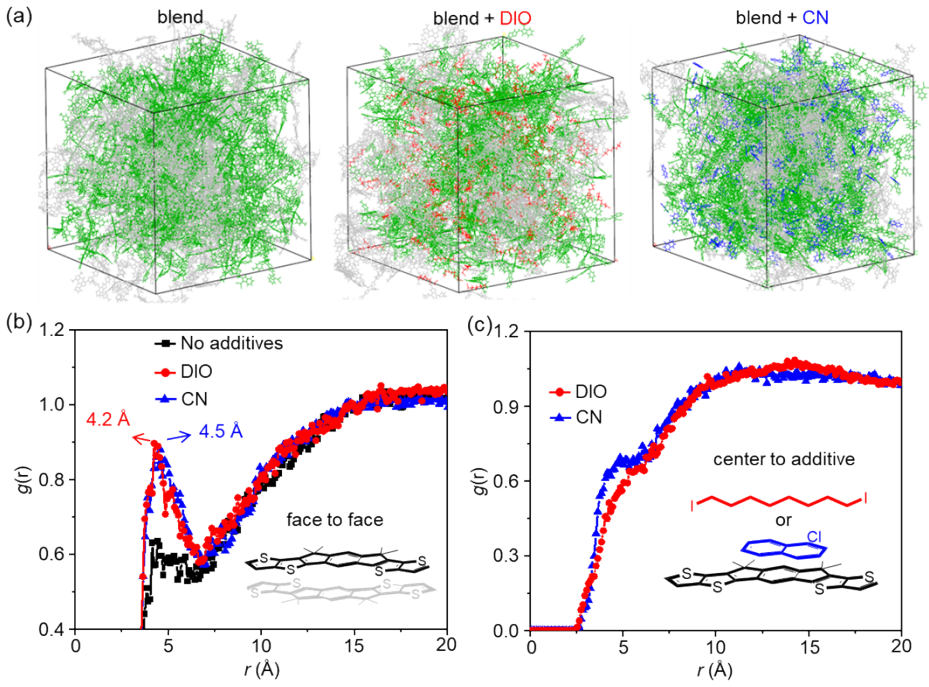

Fig. S19 (a) Snapshots from the MD results of PBDB-T:**im-ITIC**-based blend systems with different additives. (b) and (c) Radial distribution function data for blend systems with different additives.

Table S2. OSC characteristics of optimized PBDB-T:**im-ITIC**-based devices.

Run	PCE / %	J_{SC} / mA cm^{-2}	V_{OC} / V	FF / %
1	5.13	8.83	1.02	57
2	4.72	8.29	1.02	56
3	5.03	8.67	1.01	57
4	5.02	8.80	1.01	56
5	4.87	8.95	1.00	57
average	4.88 ± 0.37	8.84 ± 0.73	1.01 ± 0.01	56 ± 1

The device was fabricated using chloroform with 1 vol% of DIO as the process solvent.

Experimental details and procedures

General Information.

^{1}H and ^{13}C NMR spectra were recorded on a JEOL ECS-400 spectrometer. Data are reported as follows: chemical shift in ppm (δ), multiplicity (s = singlet, d = doublet, t = triplet, m = multiplet, br = broad), coupling constant (Hz). Mass spectra were obtained on a Shimadzu GCMS-QP-5050 or Shimadzu AXIMA-TOF. High-resolution mass spectra (HRMS) were obtained at atmospheric pressure chemical ionization (APCI) using Thermo scientific LTQ Orbitrap XL. Thermogravimetric (TGA) analysis and differential scanning calorimetry (DSC) were performed under nitrogen at a heating rate of 10 °C min^{-1} with a Shimadzu TGA-50 and a Shimadzu DSC-60, respectively. UV-vis spectra were recorded on a Shimadzu UV-3600 spectrophotometer. Emission spectra were recorded using a Fluoromax-4 spectrometer in the photocounting mode equipped with a Hamamatsu R928P photomultiplier. Differential pulse voltammetry (DPV) was carried out on a BAS CV-620C voltammetric analyzer using a platinum disk as the working electrode, platinum wire as the counter electrode, and $Ag/AgNO_3$ as the reference electrode at a scan rate of 100 mV s^{-1}. All spectra were obtained in spectrograde solvents. Photoelectron yield spectroscopy (PYS) was performed by Bunkoukeiki BIP-KV202GD. Low-energy inverse photoemission spectroscopy (LEIPS) was performed by Ulvac-Phi, Inc. LEIPS system. Atomic force microscopy (AFM) was obtained by Shimadzu SPM9600. Elemental analysis was performed on a Perkin Elmer LS-50B instrument by the Elemental Analysis Section of Comprehensive Analysis Center (CAC), SANKEN, Osaka University.

OSC device fabrication and evaluation

Organic solar cells were prepared with a structure of ITO/ZnO/active layer/MoO_3/Ag.[8] ITO-coated glass substrates were first cleaned by ultrasonication in acetone, water, and 2-propanol for 15 min, respectively. ITO-coated glass substrates were then activated by ozone treatment for 1.5 h. ZnO layer was spin-coated using the solution of zinc acetate dihydrate (99.9%, 200 mg), ethanolamine (99%, 55 μL), and 2-methoxyethanol (99.8%, 2 mL) at 4000 rpm. and baked at 200 °C for 30 min. in the air. Subsequently, the active layer was then formed by spin-coating on the ITO/ZnO electrode in a glove box. MoO_3 and Ag electrodes were evaporated on the top of active layer through a shadow mask to define the active area of the devices (0.09 cm^2) under a vacuum of 10^{-5} Pa to a thickness of 10 and 100 nm, respectively. After sealing the device from the air, the photovoltaic characteristics were measured in air under simulated AM 1.5G solar irradiation (100 mW cm^{-2}) (SAN-EI ELECTRIC, XES-301S). The current density-voltage characteristics of photovoltaic devices were measured by using a KEITHLEY 2400 source meter. The EQE spectra were measured by using a Soma Optics Ltd. S-9240. The thickness of the active layer was determined by KLA Tencor Alpha-step IQ.

SCLC measurements

Hole-only and electron-only devices were prepared with a structure of ITO/PEDOT:PSS/active layer/MoO_3/Au and ITO/ZnO/active layer/Ca/Ag, respectively.[1] The active layers of PBDB-T:im-ITIC and PBDB-T:ITIC OSCs were prepared using the optimized fabrication conditions. The carrier mobilities of these devices were calculated by the following equation:

$$J = \frac{9}{8}\varepsilon\varepsilon_0\mu\frac{V^2}{d^3}$$

where ε, ε_0, and d are the dielectric constant of the active layer, the permittivity of free space, the carrier mobility, and the measured thickness of active layer, respectively. We used the values of $\varepsilon = 3$, $\varepsilon_0 = 8.8 \times 10^{-12}$.

The fitting and calculation details for the E_{CT}

The E_{CT} value was estimated by fitting the normalized EQE spectra using following equation:

$$EQE(E) = \frac{f}{E\sqrt{4\pi\lambda_L k_B T}} exp\left(-\frac{(E_{CT} + \lambda_L - E)}{4\lambda_L k_B T}\right)$$

Where k_B is the Boltzmann's constant, T is the absolute temperature, E_{CT} is the energy of CT states, and λ_L is related to the width of the CT absorbance band, with contributions from internal/environmental reorganization and/or energetic disorder.

Single-Crystal X-ray Diffraction Analysis

Single crystals of im-ITIC were grown by the vaper diffusion method at room temperature. im-ITIC (3 mg) samples were dissolved in $CHCl_3$ (1 mL) in a 2 mL dram vial, and it were sealed by tinfoil then poked a few small holes in the tinfoil to control its diffusion speed. This vial was placed into a 20 mL dram vial containing methanol (~10 mL). The larger vial was then sealed tightly and left undisturbed at room temperature until crystal growth occurred (2 weeks).

Table S3. Crystal data and structure refinement for im-ITIC.

	im-ITIC
CCDC number	2427692
Empirical formula	C93H78Cl4N4O2S4
Formula weight	1568.17
Temperature / K	103
Crystal system	triclinic
Space group	P-1
a / Å	13.7559(2)
b / Å	22.3818(5)
c / Å	30.1984(5)
α/°	76.312(2)
β/°	84.506(1)
γ/°	74.959(2)
Volume / $Å^3$	8718.2(3)
Z	4
ρ_{calc} / mg mm^{-3}	1.195
μ / mm^{-1}	2.621
F(000)	3276
Crystal size / mm^3	0.318 ×0.165 × 0.066
2Θ range for data collection	2.176 to 75.716°
Index ranges	$-17 \leq h \leq 17, -27 \leq k \leq 20, -37 \leq l \leq 32$
Reflections collected	98009
Independent reflections	35185
Data/restraints/parameters	35185/907/2053
GooF	1.022
Final R indexes [I>2σ (I)]	$R_1 = 0.0820$, $wR_2 = 0.2437$
Final R indexes [all data]	$R_1 = 0.0895$, $wR_2 = 0.2526$
Largest diff. peak/hole / e $Å^{-3}$	1.55/−0.99

Femtosecond transient IR absorption measurements

The TA measurements were performed using a pump-probe method with a Ti:sapphire regenerative amplifier (Spectra Physics, Solstice; 90 fs pulse duration, 1 kHz repetition rate) coupled with optical parametric amplifiers (OPAs; Spectra Physics, TOPAS Prime). A 660 nm excitation pulse from the OPA (0.1 μJ per pulse, 500 Hz) was used to selectively excite the acceptor layer. The beam diameter was approximately 200 μm, corresponding to a pump fluence of 3.18 μJ mm^{-2}. For the MIR measurements, probe pulses were generated through difference frequency generation between the signal and idler beams from the OPA in an $AgGaS_2$ crystal and detected using a 128-channel linear MCT array detector (Infrared Systems Development, FPAS-0144). The frequency shift of the cyano group in the acceptors was analysed after subtracting the background signal attributed to free carrier absorption from the spectra, where the background in the narrow region was approximated as a linear baseline. The sample films for transient absorption (TA) measurements were prepared by drop-casting a chloroform solution containing ITIC, im-ITIC, and their blend with PBDB-T (1:1 by weight) onto a CaF_2 substrate. During the measurement, the film was placed in an IR cell filled with 20 torr of N_2.

Theological calculations

In the calculations, the alkyl chains in the acceptor molecules were replaced by methyl groups for simplification. In the calculation of the distribution of frontier molecular orbitals, structural optimization was calculated by density functional theory (DFT) calculations at B3LYP/6-31G(d,p). The calculations of energy levels for different dimers and the time-dependent DFT (TD-DFT) for D:A clusters were performed by the long-range corrected (LRC) functional ωB97XD and 6-31G(d,p) basis set.

Molecular-dynamics (MD) simulations

The MD simulations were performed with the Gromacs 2024.2 software package based on the general AMBER force field (GAFF) with the RESP charges.[2-5] The Berendsen method was applied for the control of pressure, and the velocity rescaling method with a stochastic term (v-rescale) was applied for the control of temperature. All covalent hydrogen bonds were constrained using the LINCS algorithm and a cutoff range for the short-range electrostatics was set to 13 Å. For im-ITIC and ITIC, the molecular geometry was optimized at B3LYP/6-31G(d,p) level. For PBDB-T, 10 repeat units were used as a fragment of the polymer, then the molecular geometry was optimized at B3LYP/6-31G level. For pristine system, the initial cell was built by randomly placing total 200 molecules of im-ITIC or ITIC and 200 fragments of DIO or CN in a 20 × 20 × 20 nm^3 cubic box to generate an initial geometry. For blend system, 30 fragments of PBDB-T, 200 fragments of im-ITIC or ITIC and 200 fragments of DIO or CN were randomly placed in a 30 × 30 × 30 nm^3 cubic box to generate an initial geometry. The simulation was carried out using the following procedure:[6,7] (1) 5 ns of simulation at 800 K and 100 bar to make molecules close together quickly; (2) 10 ns of simulation at 800 K and 1 bar, then cooling down to 300 K in 10 ns; (3) 30 ns of equilibration at 300 K and 1 bar for production. The final results were the average of three

independent simulations. Radial distribution functions (RDF) were computed using the TRAVIS program.[8]

Preparation of materials

Commercially available reagents were used without purification. All reactions were carried out under a nitrogen atmosphere. Compounds **1** were prepared by the reported procedures.[9]

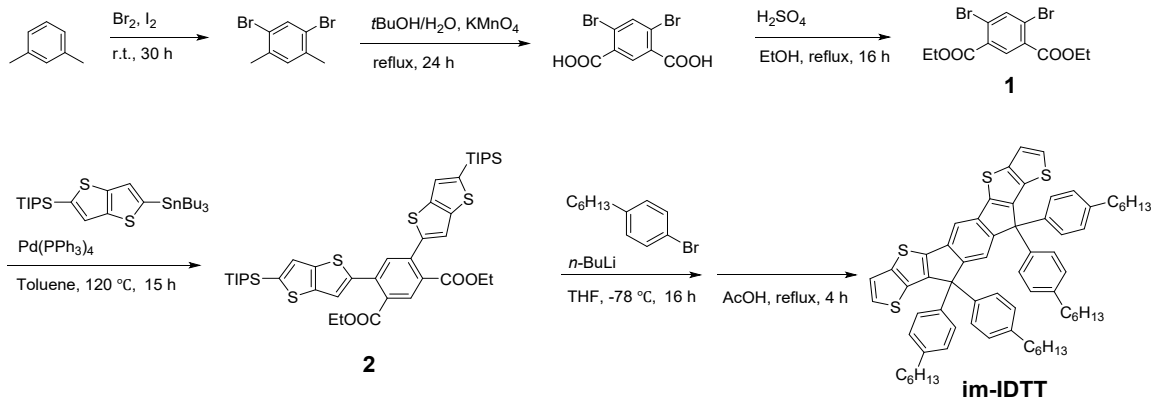

Scheme S1. Synthetic route of compounds **im-IDTT**

Synthetic procedures and characterizations

Synthesis of diethyl 4,6-bis(5-(triisopropylsilyl)thieno[3,2-b]thiophen-2-yl)isophthalate (**2**): Compound 1 (0.9 g, 2.4 mmol), triisopropyl(5-(tributylstannyl)thieno[3,2-b]thiophen-2-yl)silane (3.5 g, 6.0 mmol), and $Pd(PPh_3)_4$ (138 mg, 0.12 mmol) were dissolved in 30 mL of toluene under inert atmosphere. The mixture was heated to 120 °C and stirred for 15 h. After the reaction, the system was allowed to cool to room temperature and then concentrated under reduced pressure. The crude product was purified by column chromatography on silica gel using *n*-hexane/chloroform (1:2) as eluent, yielding compound **2** as a yellow solid (1.6 g, 83%). ^{1}H NMR (400 MHz, $CDCl_3$): δ (ppm) 8.15 (s, 1H), 7.70 (s, 1H), 7.35 (s, 2H), 7.28 (s, 2H), 4.29-4.24 (m, 4H), 1.39-1.32 (m, 6H), 1.18-1.11 (m, 36H), 0.93-0.89 (t, J = 7.24 Hz, 6H).

Synthesis of **im-IDTT**: To a solution of 1-bromo-4-hexylbenzene (3.1 mL, 15.3 mmol) in THF (20 mL) at –78 °C, *n*-butyllithium solution (1.56 M in *n*-hexane, 9.9 mL, 15.3 mmol) was added dropwise and stirred for 1 H. The solution was kept at –78 °C, and a solution of compound **2** (1.6 g, 2.0 mmol) in THF (50 mL) was added dropwise. The mixture was slowly warmed up to room temperature and stirred for 16 h and then quenched by water. The solution was extracted by $CHCl_3$ and washed with water and brine. The organic phase was concentrated and purified by column chromatography on silica gel using *n*-hexane/$CHCl_3$/EtOAc (10/2/1, v/v/v) as an eluent to give 2a as yellow solid (1.6 g, 60%). This compound was subjected immediately to a solution of 50 mL acetic acid with 1 mL of concentrated sulfuric acid, and reflux for 4 h. After reaction, the mixture was washed with water and extracted by $CHCl_3$. The organic phase was concentrated and purified by column chromatography on silica gel using *n*-hexane/$CHCl_3$ (4/1, v/v) as an eluent to give **im-IDTT** as light orange solid (683 mg, 57%). ^{1}H NMR (400 MHz, $CDCl_3$): δ (ppm) 7.52 (s, 2H), 7.30-7.27 (m, 4H), 7.09-7.07 (d, J = 8.59 Hz, 8H), 6.97-6.95 (d, J = 8.59 Hz, 8H), 2.50-2.47 (m, 8H), 1.53-1.48 (m, 8H), 1.29-1.26 (m, 24H), 0.86-0.83 (t, J = 6.79 Hz, 12H). ^{13}C NMR (100 MHz,

$CDCl_3$) δ: 151.41, 146.38, 142.85, 141.95, 141.65, 140.38, 137.53, 133.98, 128.34, 127.96, 126.67, 124.25, 120.45, 109.85, 63.13, 35.64, 31.80, 31.48, 29.24, 22.71, 14.19. HRMS (APCI) m/z calcd. for $C_{68}H_{75}S_4$ $[M + H]^+$: 1019.4673; found: 1019.4755 . Elemental Anal. Calcd. for $C_{68}H_{74}S_4$: C 80.11, H 7.32, N 0.00; found: C 80.05, H 7.19, N 0.00.

Synthesis of ***im-IDTT-CHO***: **im-IDTT** (300 mg, 0.29 mmol) was placed in a two-necked flask and dissolved in THF (25 mL). Lithium diisopropylamide (5.88 mL, 1.0 M in THF/*n*-hexane) was added to the mixture at –78 °C. After stirring for 1 h at the temperature, *N*,*N*-dimethylformamide (0.9 mL, 11 mmol) was added. The mixture was gradually warmed up to room temperature and stirred for 12 h. The reaction was quenched by water and extracted by $CHCl_3$. After removal of the solvent under reduced pressure, the crude product was purified by column chromatography on silica gel using *n*-hexane/$CHCl_3$ (3/1, v/v) as an eluent to give **im-IDTT-CHO** as orange solid (277 mg, 88%). This compound was subjected immediately to the next reaction without further purification. ^{1}H NMR (400 MHz, $CDCl_3$): δ (ppm) 9.88 (s, 2H), 7.95 (s, 2H), 7.66 (s, 1H), 7.62 (s, 1H), 7.05-7.03 (d, *J* = 8.36 Hz, 8H), 6.99-6.97 (d, *J* = 8.29 Hz, 8H), 2.51-2.47 (m, 8H), 1.53-1.48 (m, 8H), 1.31-1.26 (m, 24H), 0.87-0.83 (t, *J* = 6.79 Hz, 12H).

Synthesis of ***im-ITIC***: Pyridine (0.5 mL) was added to the solution of ***im-IDTT-CHO*** (100 mg, 0.093 mmol) and 3-(dicyanomethylidene)indan-1-one (108 mg, 0.56 mmol) in $CHCl_3$ (15 mL) and the resulting mixture was stirred at 75 °C for 12 h. The reaction mixture was washed with water 3 times and the organic phase was concentrated. The crude product was purified by column chromatography on silica gel using *n*-hexane/$CHCl_3$ (2/1 to 1/2, v/v) as eluent, followed by further purification with reprecipitation using $CHCl_3$ and acetone to give **im-ITIC** as deep blue solid (96 mg, 72%). ^{1}H NMR (400 MHz, $CDCl_3$) δ: 8.66 (s, 2H), 8.61-8.59 (m, 2H), 7.93-7.91 (m, 2H), 7.84 (s, 2H), 7.76-7.73 (m, 4H), 7.63 (s, 1H), 7.49 (s, 1H), 7.17-7.15 (d, *J* = 8.41 Hz, 8H), 6.99-6.97 (d, *J* = 8.29 Hz, 8H), 2.55-2.51 (m, 8H), 1.53-1.50 (m, 8H), 1.32-1.25 (m, 24H), 0.85-0.82 (t, *J* = 6.50 Hz, 12H). ^{13}C NMR (100 MHz, $CDCl_3$) δ: 188.15, 159.64, 154.86, 152.51, 147.26, 146.67, 143.32, 142.71, 139.92, 139.24, 138.98, 137.81, 137.04, 136.82, 136.54, 135.25, 134.74, 128.92, 127.90, 125.22, 124.09, 122.33, 114.58, 114.25, 112.00, 69.37, 63.86, 35.65, 31.78, 31.54, 29.25, 22.71, 14.18. HRMS (APCI) m/z calcd. for $C_{94}H_{83}N_4O_2S_4$ $[M]^+$: 1428.5354; found: 1428.5428. Elemental Anal. Calcd. for $C_{94}H_{82}N_4O_2S_4$: C 79.07, H 5.79, N 3.92; found: C 78.78, H 5.89, N 3.84.

NMR spectra

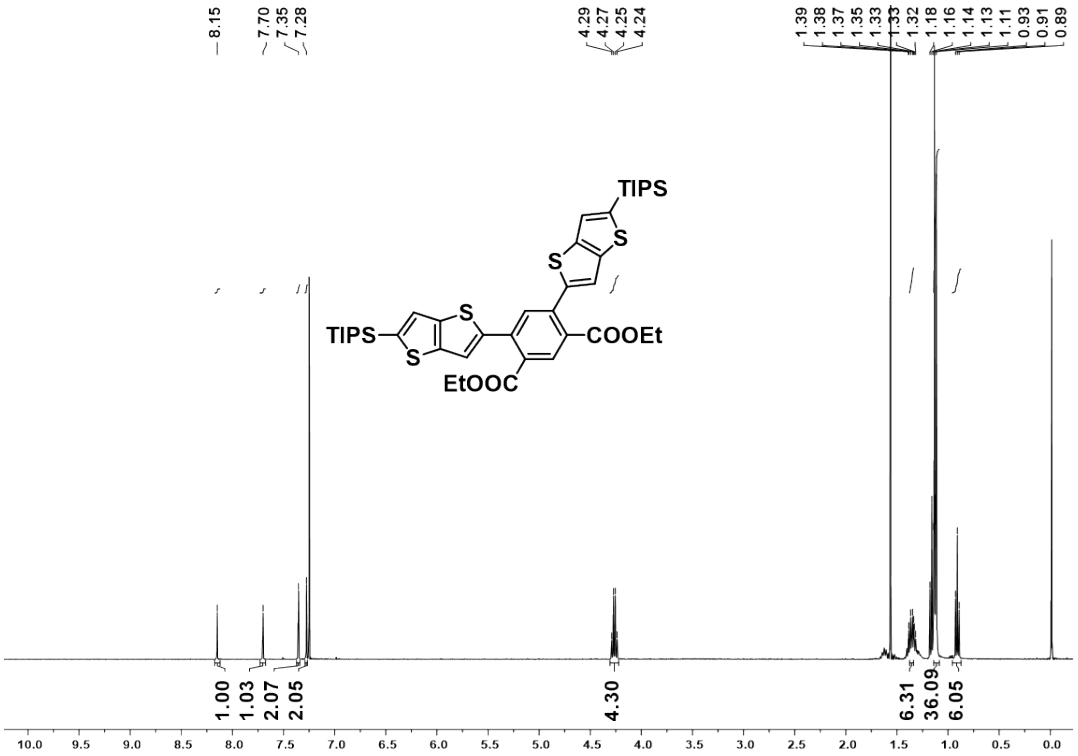

Fig. S20. ^{1}H NMR spectrum of **2** in $CDCl_3$.

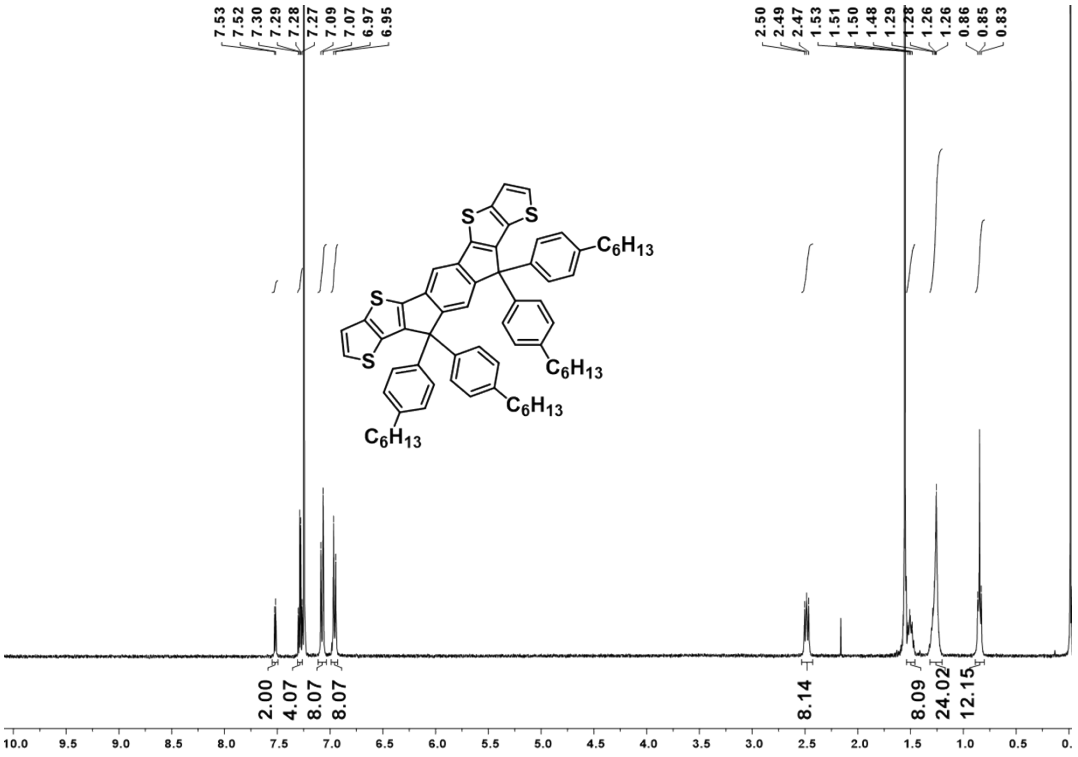

Fig. S21. ^{1}H NMR spectrum of **im-IDTT** in $CDCl_3$.

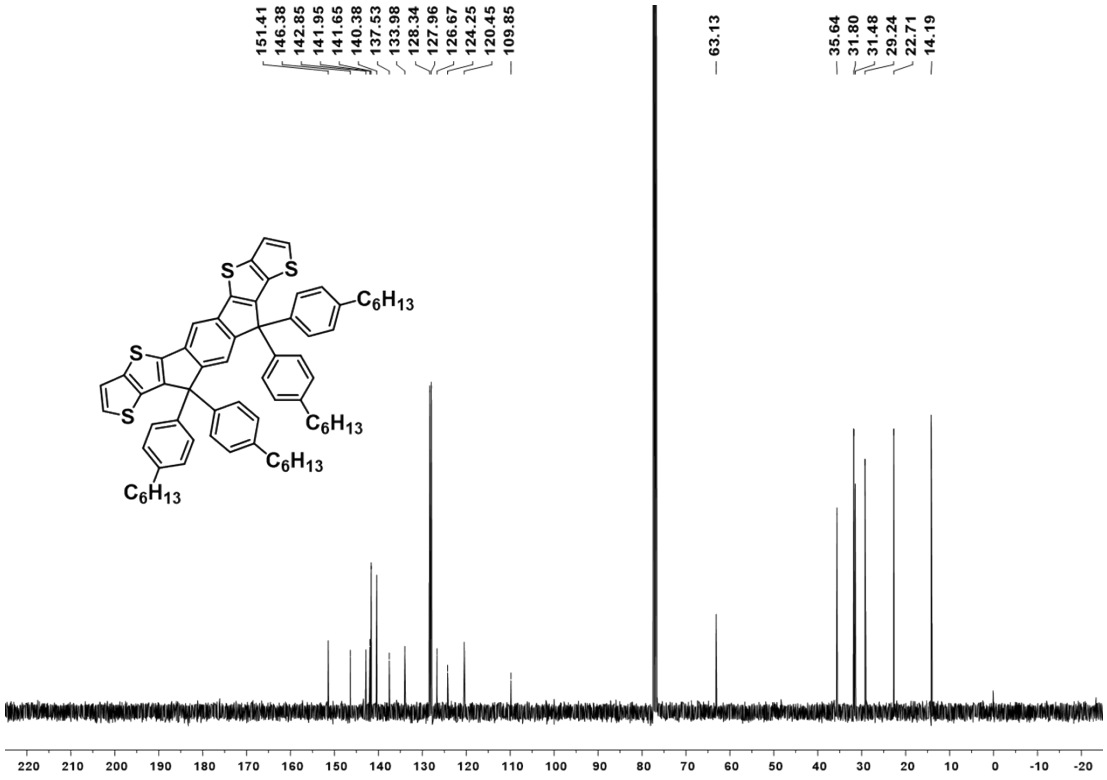

Fig. S22. ^{13}C NMR spectrum of **im-IDTT** in $CDCl_3$.

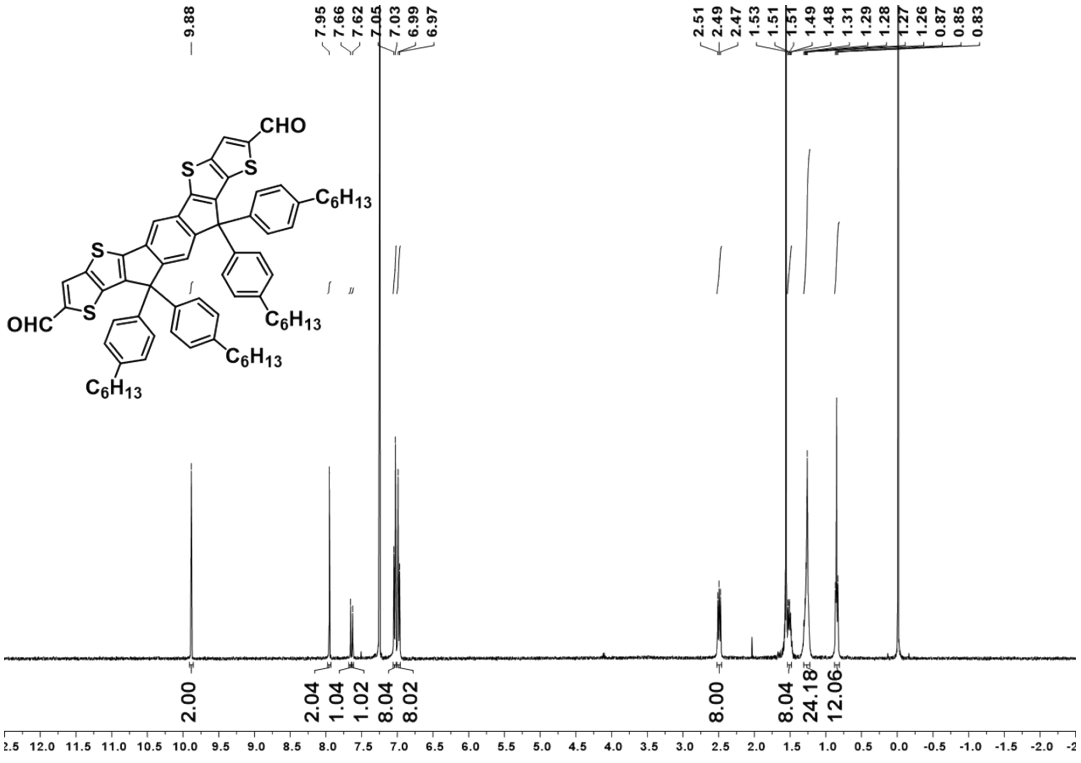

Fig. S23. ^{1}H NMR spectrum of **im-IDTT-CHO** in $CDCl_3$.

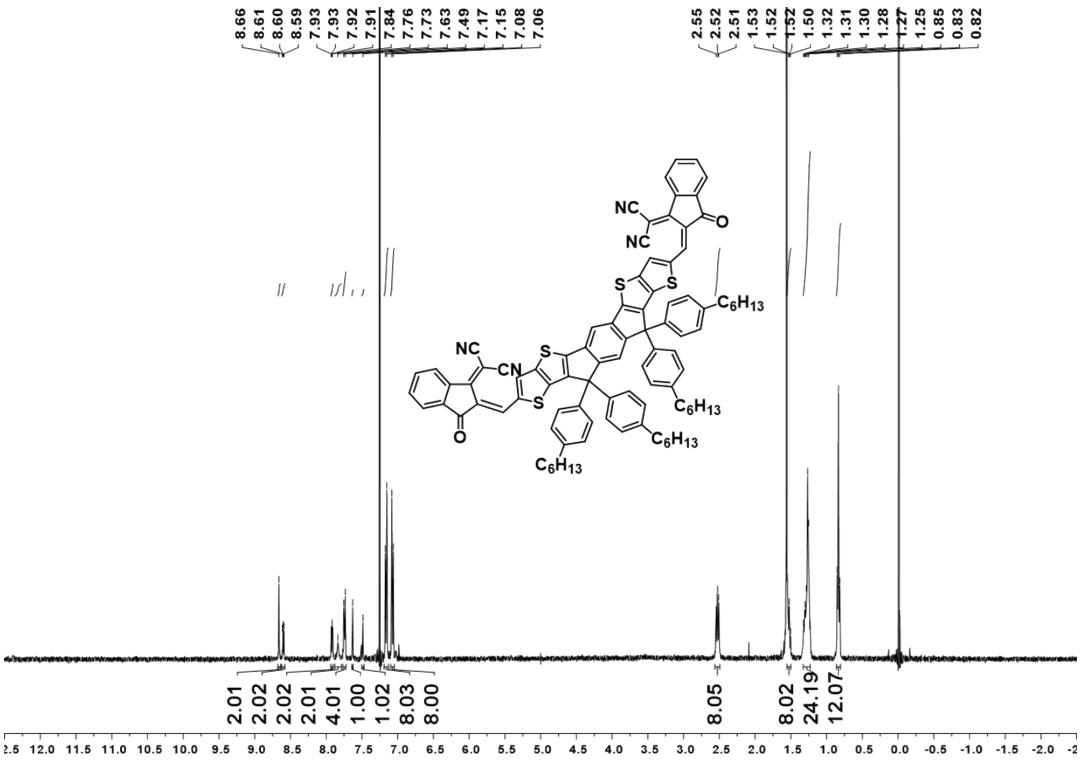

Fig. S24. ^{1}H NMR spectrum of **im-ITIC** in $CDCl_3$.

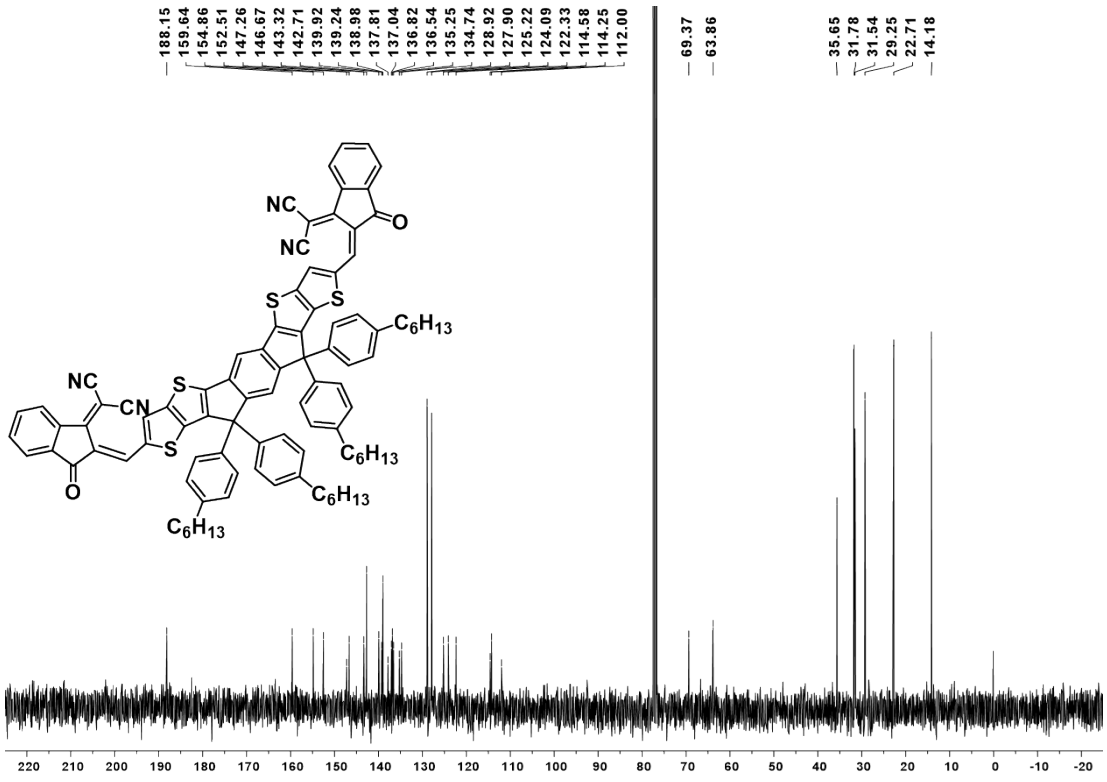

Fig. S25. ^{13}H NMR spectrum of **im-ITIC** in $CDCl_3$

References

1 S. Jinnai, K. Murayama, K. Nagai, M. Mineshita, K. Kato, A. Muraoka, A. Yamakata, A. Saeki, Y. Kobori and Y. Ie, *J. Mater. Chem. A*, 2022, **10**, 20035-20047.

2 C. I. Bayly, P. Cieplak, W. D. Cornell and P. A. Kollman, *J. Phys. Chem.*, 1993, **97**, 10269-10280.

3 J. M. Wang, R. M. Wolf, J. W. Caldwell, P. A. Kollman and D. A. Case, *J. Comput. Chem.*, 2004, **25**, 1157-1174.

4 T. Lu and F. W. Chen, *J. Comput. Chem.*, 2012, **33**, 580-592.

5 B. Hess, C. Kutzner, D. van der Spoel and E. Lindahl, *J Chem. Theory Comput.*, 2008, **4**, 435-447.

6 L. Ye, H. W. Hu, M. Ghasemi, T. H. Wang, B. A. Collins, J. H. Kim, K. Jiang, J. H. Carpenter, H. Li, Z. K. Li, T. McAfee, J. B. Zhao, X. K. Chen, J. L. Y. Lai, T. X. Ma, J. L. Bredas, H. Yan and H. Ade, *Nat. Mater.*, 2018, **17**, 253-260.

7 Y. K. Li, Y. Guo, Z. Chen, L. L. Zhan, C. L. He, Z. Z. Bi, N. N. Yao, S. X. Li, G. Q. Zhou, Y. P. Yi, Y. Yang, H. M. Zhu, W. Ma, F. Gao, F. L. Zhang, L. J. Zuo and H. Z. Chen, *Energy Environ. Sci.*, 2022, **15**, 855-865.

8 M. Brehm, M. Thomas, S. Gehrke and B. Kirchner, *J. Chem. Phys.*, 2020, **152**, 164105.

9 T. K. Pal, S. Neogi and P. K. Bharadwaj, *Chem. Eur. J.*, 2015, **21**, 16083-16090.